 doi:10.20944/preprints202203.0373.v1

Article

Preliminary Statistical Characterizations of the Lowest Kilometer Time-Height Profiles of the Rainfall Rate Using a Vertically Pointing Radar

A. R. Jameson [1,*] and M. L. Larsen [2]

[1] RJH Scientific, Inc., arjatrjhsci@gmail.com
[2] College of Charleston, Department of Physics, larsenml@cofc.edu
* Correspondence: arjatrjhsci@gmail.com

Abstract: A realistic approach for gathering high-resolution observation of the rainfall rate, *R*, in the vertical plane is to use data from vertical pointing Doppler radars. After accounting for the vertical air velocity and attenuation, it is possible to determine the fine, spatially resolved drop size spectra and to calculate *R* for further statistical analyses. The first such results in a vertical plane are reported here. Specifically, we present results using MRR-Pro Doppler radar observations at resolutions of ten meters in height over the lowest 1.28 km as well as ten seconds in time over four sets of observations using two different radars at different locations. Both correlation functions and power spectra are useful for translating observations and numerical model outputs of *R* from on one scale down to other scales that may be more appropriate to particular applications such as flood warnings and soil erosion, for example. However, it was found in all cases that while locally applicable radial power spectra could be calculated, because of statistical heterogeneity, most of the power spectra lost all generality and proper correlation functions could not be computed in general except for one 17 minute interval. Nevertheless, these results are still useful since they could be combined to develop catalogs of power spectra over different meteorological conditions and in different climatological settings and locations. Furthermore, even within the limitations of these data, this approach is being used to gain a deeper understanding of rainfall to be reported in a forthcoming paper.

Keywords: raindrop size distributions (DSD) from Doppler radar; computing radial power spectra using radar Doppler spectra; vertical pointing Doppler rain observations

1. Introduction

Correlation functions and power fits to spectral powers have been used extensively to relate measurements of rainfall rates at different temporal and spatial scales (e.g., [1]-[-5] and many others). However, such studies have concentrated exclusively on the horizontal dimensions and time because of the difficulty of measuring rainfall rate in the vertical especially at high resolution over any significant depth. This study is a first step toward addressing this deficiency.

This is achieved by using vertical observations in rain using the Micro-Rain Radar (MRR) that is a continuous wave Doppler radar operating at a wavelength of 1.24 cm as described in detail in [6]. It has selectable vertical resolutions, integration times and sampling intervals. In this study, we use a vertical resolution of 10 meters over a depth of 1.28 km and with 10 s integration and 64 point Doppler spectra over an unambiguous Doppler velocity range of approximately 12 m s^{-1}.

These measurements are affected by both attenuation by the rain and the vertical air velocity which can distort the raindrop size spectra and the estimated drop concentrations used to calculate the rainfall rates and other parameters. Both effects can be taken into account and corrected as described in detail in [7]. The lengthy discussions therein will

 doi:10.20944/preprints202203.0373.v1

not be repeated here except to say that the approach uses velocity shifted Doppler spectra until the observed and theoretical powers agree. Furthermore, we emphasize that this is not a work about what has been done in the past using the MRR particularly in snow, for example, nor how to use that radar, but rather the focus here is on an interesting first atmospheric application in rain that will be expanded upon further in a future study already under preparation and that will be described in greater detail at the end of this present work.

However, there is no guarantee that the tools of proper correlation functions and power fits will always exist. In particular the correlation function exists only when they are independent of the origin of the calculation in space or time over the spatial-temporal domain of interest. Similarly, power spectra, whether power fits or otherwise, only have generality when the data are wide-spread statistically homogeneous and statistically stationary (WSS) as emphasized for the rainfall rate in [8]).

Specifically, then, the first order of business is to see whether or not the temporal-vertical MRR observations of the rainfall rates are statistically homogeneous. There are two components to this determination. First, at all times and in all directions, there has to be only one global mean value. Second, the variance must be the same at all times and in all directions as well. In order to address the first requirement, the method of inverting individual observations is used to look at the distributions of the mean values ([8]-[11]). When there is a unitary peak in the resulting distribution, this condition is satisfied. It should be noted, however, that while an entire data set may not satisfy these conditions, they may be locally satisfied. Whether or not these local regions are useful remains to be seen.

The variance requirement is addressed using the results of Anderson and Kostinski ([12]-[13] through the analysis of the difference in the number of sequential maxima and minimum forward and backward directions in a string of data denoted by the variable $\alpha = T_{\text{foreward}} - T_{\text{backward}}$ where T is the total count of record highs and record lows in each direction. For a sample size greater than ten, α is normally distributed with a null mean and standard deviation σ_α dependent on the sample size (Figure1 in [14]). Asymmetries in the variance will then appear as non-zero mean α of a magnitude that can then be statistically evaluated with respect to σ_α. An example of these applications to MRR data are provided in the next section with the analyses results for four different sets of data provided subsequently.

While some argue that these two requirements are 'too restrictive' for real rain, those, unfortunately, are the mathematical requirements for WSS. Furthermore, because the data analyzed here are along two orthogonal dimensions, one must apply both criteria in both directions to evaluate the appropriateness of WSS over the area.

2. Examples of the data processing for determining statistical homogeneity for time-height rainfall rate data

2.1. Convective, variable rain

Figure1 is a plot of the time height MRR vertical air velocity, attenuation corrected rainfall rates using observations which were collected by one of the MRR radars as part of a National Science Foundation project and operated by the College of Charleston located near Charleston, South Carolina. It is located on property owned by the College of Charleston Foundation that is used for a variety of ecological, educational, and research purposes (e.g., see [15]). The methodology for the correction of the data for vertical air velocity and attenuation is as explained in [7]. As one would expect for this time of year in South Carolina, the rain is associated with convection having a wide-range of rainfall rates. The most noticeable feature overall is the vertical structure of the rain that, of course, is not surprising in convective rain.

Preprints (www.preprints.org) | NOT PEER-REVIEWED | Posted: 29 March 2022 doi:10.20944/preprints202203.0373.v1

However, it does suggest that the determination of statistical homogeneity will have a strong dependency on direction. Since truly statistically homogeneous data is independent of direction of measurement, this means that any regions of such data would be those locations where the calculations of statistical homogeneity in both the vertical and the horizontal directions overlap.

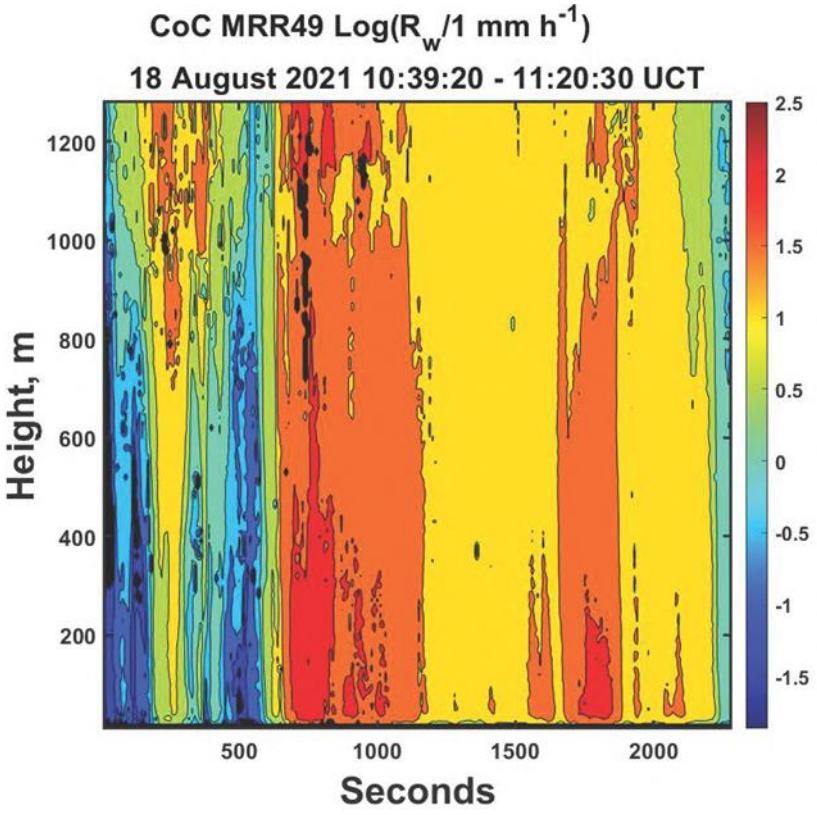

Figure 1. Time-height plot of the base 10 logarithm of the vertical air velocity corrected Doppler spectra rainfall rate from one of the College of Charleston MRR radars illustrating rain shafts typical of summer convective rain there. Areas of black denote missing data.

Specifically, to explore each direction an optimal way of looking at the two-dimensional data is to stack each column to form two, one dimensional arrays, one for time and one for the vertical dimension, as discussed on p. 1406 in [14]. A local regression mean curve (a least square error fit over twice the decorrelation length) is then fit to these data and the deviations from the mean gives the fluctuations used in the subsequent analyses using α. The results are illustrated in Figure2a for the temporal dimension and in Figure2b for the vertical direction. Obviously, there are significant differences between the two. The grey horizontal lines largely correspond to symmetrical regions in the fluctuations so that α should be relatively constant. These regions are then used in the analyses. The blue line in Figure2b highlight the ever changing values of the fluctuations so that α would also be ever changing. Hence the entire region is selected as one block of data as indicated by the extended grey line.

Preprints (www.preprints.org) | NOT PEER-REVIEWED | Posted: 29 March 2022 doi:10.20944/preprints202203.0373.v1

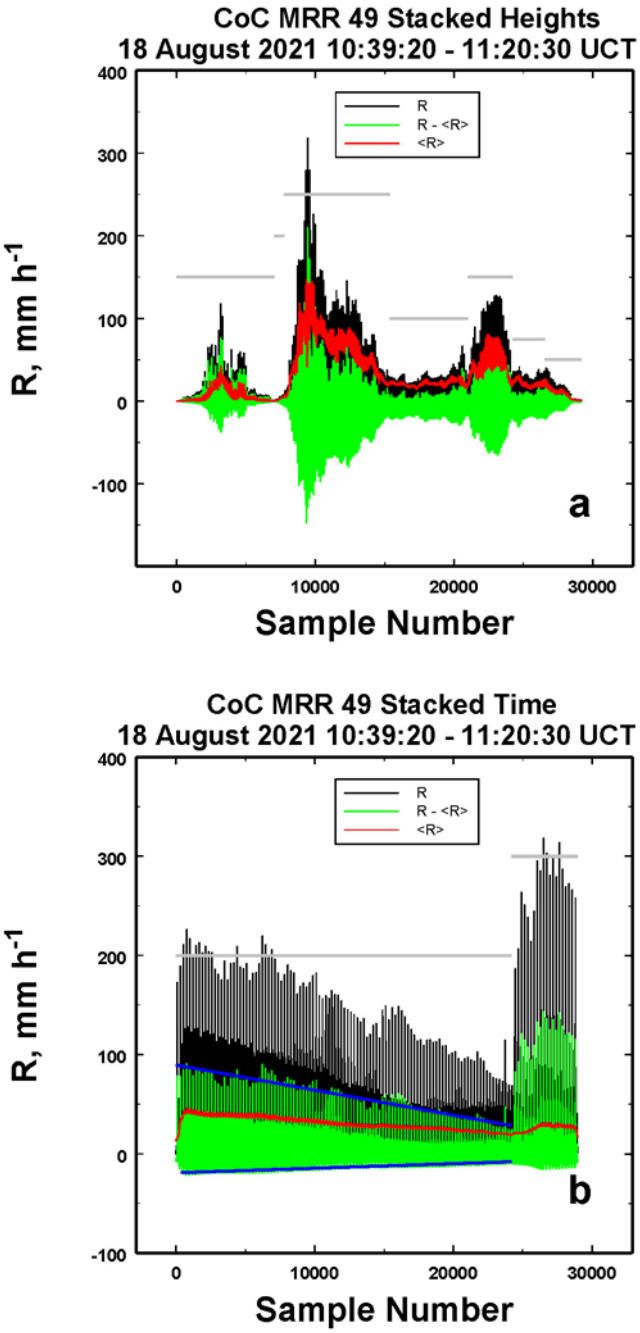

Figure 2. Data series constructed from (a) stacking the sequential observations in height in Figure 1 into a single vector (black lines) with the computed mean curve (red) and fluctuations (green) and (b) from stacking sequential time observations over all time. As explained in the text, the grey lies denote the breakdown into regions for subsequent calculations of the statistical homogeneity *IXH*. In (b) the blue line indicates where the fluctuations are constantly changing.

The more symmetric region of fluctuations is identified by the second grey line.In each of these sections, the Bayesian analysis is performed to determine the numbers of contributing mean value components (N_b). In addition, the α analyses were performed separately to yield the α relative dispersion $RD_\alpha = |\alpha| / \sigma_\alpha$ where $|\alpha|$ is the absolute value of α and σ_α is the standard deviation of α given by

$$\sigma_\alpha = \left[4ln(n) - 4.271\right]^{1/2} \quad (1)$$

Preprints (www.preprints.org) | NOT PEER-REVIEWED | Posted: 29 March 2022 doi:10.20944/preprints202203.0373.v1

where n is the number of measurements in the string of observations (from Jameson et al. 2018). In that same article , an index of statistical homogeneity is then defined to be the combination of these two factors namely,

$$IXH = \frac{1}{2}\left[H\left(\frac{RD_\alpha}{1.5} - 1\right)\left(\frac{RD_\alpha}{1.5} - 1\right) + \left(N_b - 1\right)\right] \quad (2)$$

where H is the Heaviside unit step function requiring RD_α to exceed 1.5. We refer that term to the alpha factor and the second term is the number of mean values (Bayesian) factor. In purely statistically homogeneous data, $\alpha = 0$ and $N_b = 1$ so that IXH = 0. In reality, these are very restrictive conditions rarely seen in real data so that we use IXH $\leq$ 0.5 to be a sufficient indication of statistical homogeneity.

In truly statistically homogeneous conditions, all results should be the same for the temporal and vertical directions. Obviously, in general that is not the case for these data, but it does not rule out local regions where such equivalence may be approximately valid as suggested by Figure 3 which are plots of the average values over the combined results across the sample numbers over the temporal and vertical directions. The shaded regions are where the data would be statistically homogeneous. By and large the fluctuations never satisfy the requirement for statistical homogeneity except beyond about sample number 2500. While there are a few more locations where the mean value factor is satisfactory, it is only beyond about sample number 2600 when all the conditions for statistical homogeneity are met.

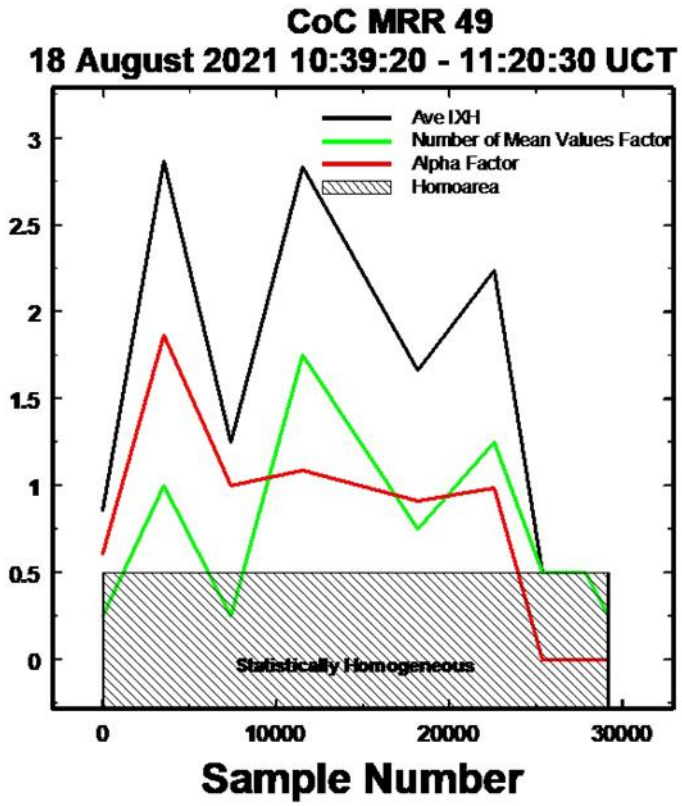

Figure 3. Plots of the *IXH* averaged over the temporal and height vector series for each of the grey areas in Figure2 placed at the mid-points of each region. Only at the right-most part of the figure is there any sign of statistical homogeneity.

To see where in space and time these conditions are met, we first interpolate the IXH values in the space series and in time series separately. These are then unstacked to return

Preprints (www.preprints.org) | NOT PEER-REVIEWED | Posted: 29 March 2022 doi:10.20944/preprints202203.0373.v1

them to their original time-height locations, and finally, these are then averaged together to estimate a combined field. We then impose two requirements for statistical homogeneity on the resulting field of data. The first is that IXH ≤ 0.5, and the second is that in those locations satisfying this first requirement, the absolute value of the difference between the two fields for each direction separately be ≤ 0.3. This latter requirement is designed to satisfy the directional independence of statistical homogeneity.

The results are illustrated in Figure 4 where the contours of shading indicate where statistical homogeneity is possible (brighter areas) and where it is not (darker areas) are over laid on the rainfall rates. The first obvious feature is that with the exception of a tiny narrow region at the top-left, these data are all statistically heterogeneous.

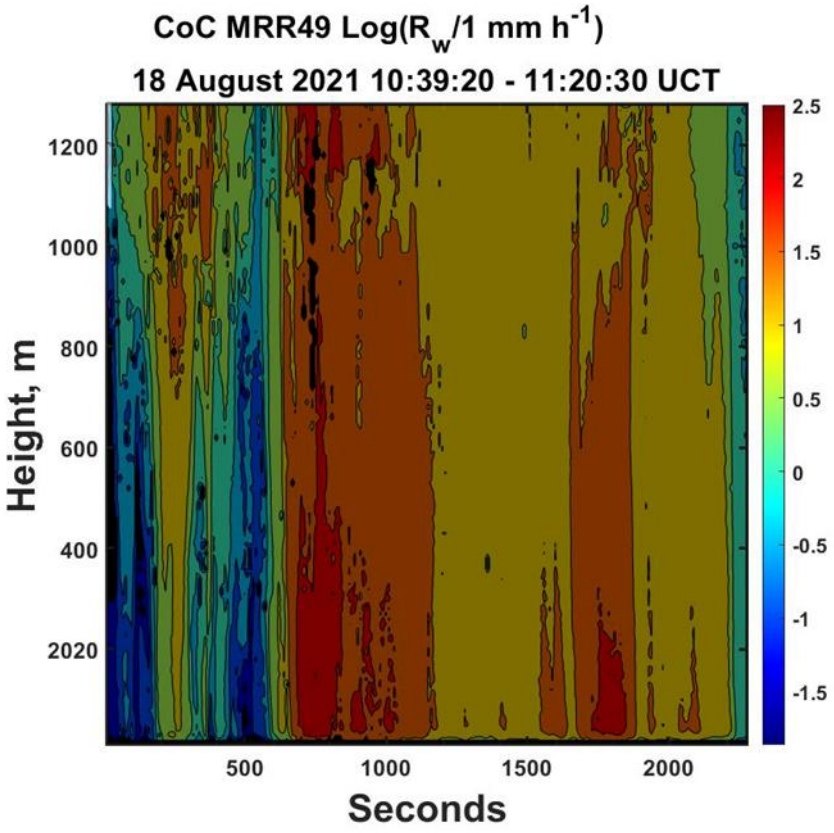

Figure 4. A replot of Figure 1 with an overlay of the height and time 2-D *IXH*. Lighter areas denote where there is statistical homogeneity subject to the two requirements discussed in the text, while the darker areas denote where there is only statistical heterogeneity. For this set of observation, there is only one narrow region of statistically homogeneous data in the top left.

To see whether these results also apply to other data, we next consider three more sets of data all from June 3, 2019 and measured using a NASA MRR-Pro radar located at the Wallop's Island Flight Facility. The rainfall rates have already been previously determined as explained in [7]).

These observations were broken into three segments denoted as early, middle and later pieces. The rainfall rates and the analysis results for the early period are shown in Fiure.5 . Because of the profound convective nature of this part of the storm with widely varying rainfall rates over short times, there were no locations of any statistical homogeneity in a manner quite similar to the previous case.

Preprints (www.preprints.org) | NOT PEER-REVIEWED | Posted: 29 March 2022 doi:10.20944/preprints202203.0373.v1

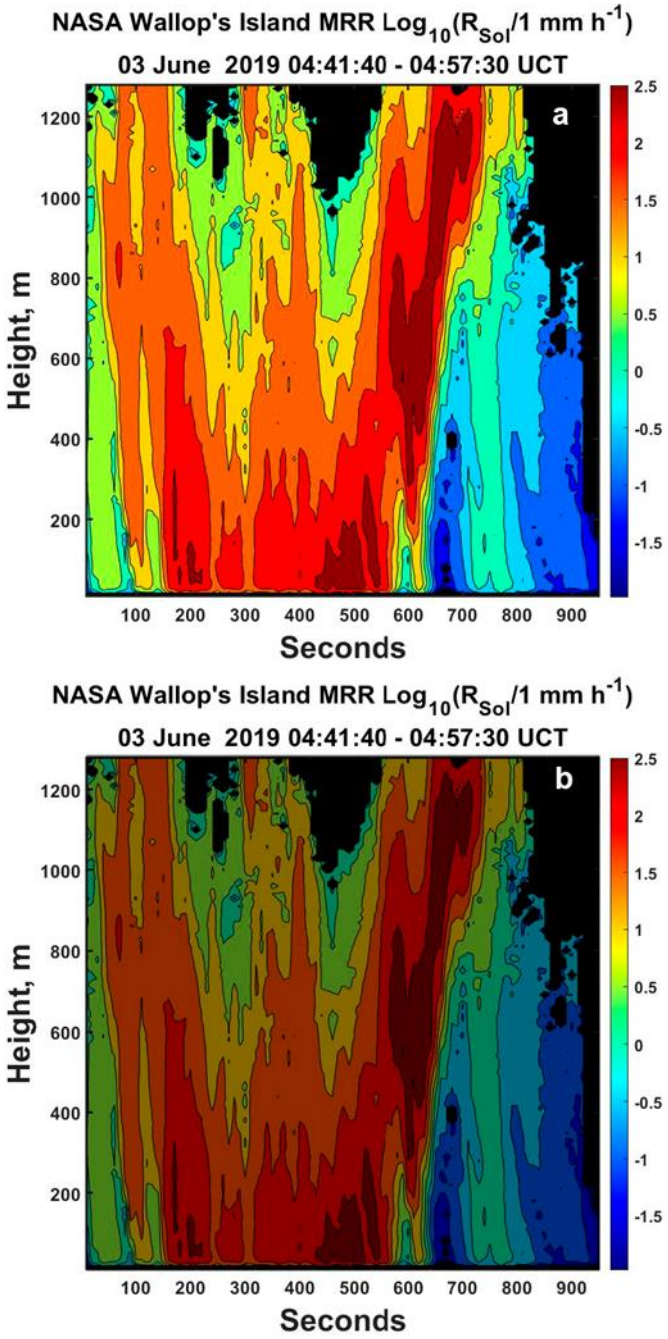

Figure 5. (a) Time-height plot of the base 10 logarithm of the vertical air velocity corrected Doppler spectra rainfall rate using data from a NASA Wallop's Island MRR radar (from [7]) during the passage of a line of convection and (b) the same plot with the overlay of the 2D *IXH* results. Note that this time there are no regions of statistical homogeneity apparently because of the variability of R_w in both height and time.

However, even during the middle period of much lighter precipitation only a few small regions of statistical homogeneity were found at times in the lower few hundred meters as plotted in Figure 6.

Preprints (www.preprints.org) | NOT PEER-REVIEWED | Posted: 29 March 2022 doi:10.20944/preprints202203.0373.v1

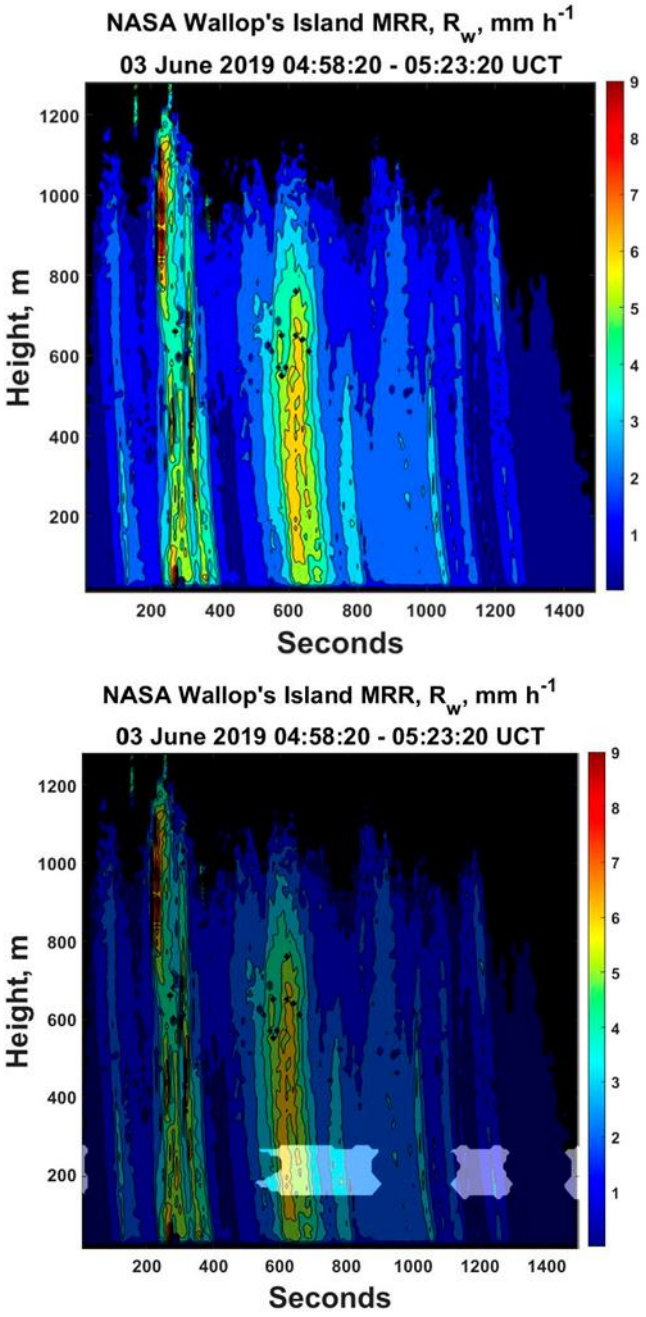

Figure 6. Similar to Figure .5 except for a the subsequent 25 minutes. This time there are larger areas of statistically homogeneity but still they are confined and found only at locations below 300 m height.

During the later time period, there was a region of light rainfall followed by a period of more intense rain as shown in Figure 7a. In this later period, there were a few larger regions of statistically homogeneous data, but still, by and large, the rainfall rates remain statistically heterogeneous.

The result is that for all four of these convective rainfalls, the data must be considered to be statistically heterogenous. This means that correlation functions in time and height do not exist. In so far as these data are representative of typical convective rain, it also seems plausible that this will be true for most convective rain. What happens in steadier, more stratiform rain remains to be determined.

Preprints (www.preprints.org) | NOT PEER-REVIEWED | Posted: 29 March 2022 doi:10.20944/preprints202203.0373.v1

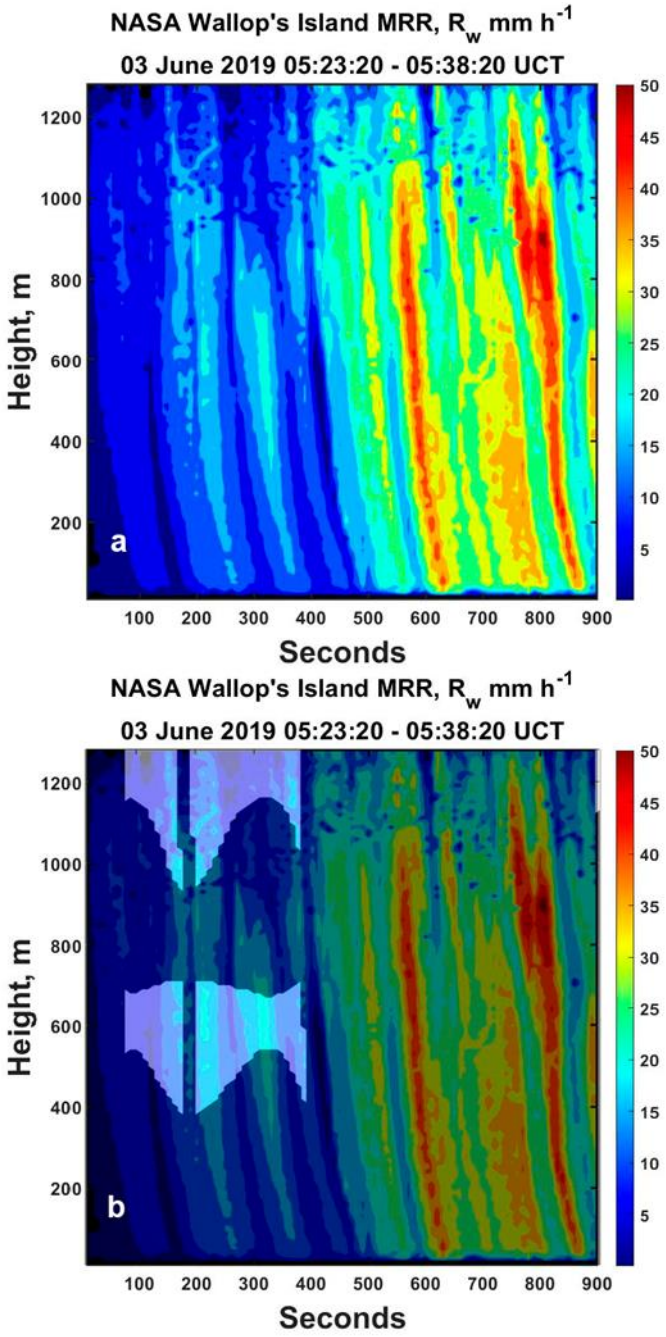

Figure 7. Similar to the previous figures except for the final sequential 15 minutes that begins with lighter rain followed by regions where the rainfall is more intense. Some expanded locations of statistically homogeneous rain are found in the locations of less intense rain, but they are still rather isolated in both dimensions (adapted from Jameson et al. 2021).

Thus, correlation functions are usually likely to be of little use when trying to tranform rainfall rate among different time and/or different spatial scales. Nor can they be transformed into power spectra with any general applicability(e.g., see [8]) via the Wiener-Khintchine theorem [16,17]. However, the power spectra of these data fields might still serve a useful albeit more narrow purpose.

To explore further and until we have access to two dimensional spatial data, then, the temporal axis is converted into a spatial coordinate by assuming an advection velocity of 1 m s^{-1}. This yields horizontal dimensions (i.e., 900 – 1490 m) for the NASA MRR data and up to 2280 m for the College of Charleston MRR 49 observations with all having a

Preprints (www.preprints.org) | NOT PEER-REVIEWED | Posted: 29 March 2022 doi:10.20944/preprints202203.0373.v1

vertical distances of 1280 m. In each case, the rainfall rate data are then Fourier processed to yield the two-dimensional power spectra which can then be transformed into the one-dimensional spectra in height and in the horizontal (time) for each period. These are illustrated in Figure 8.

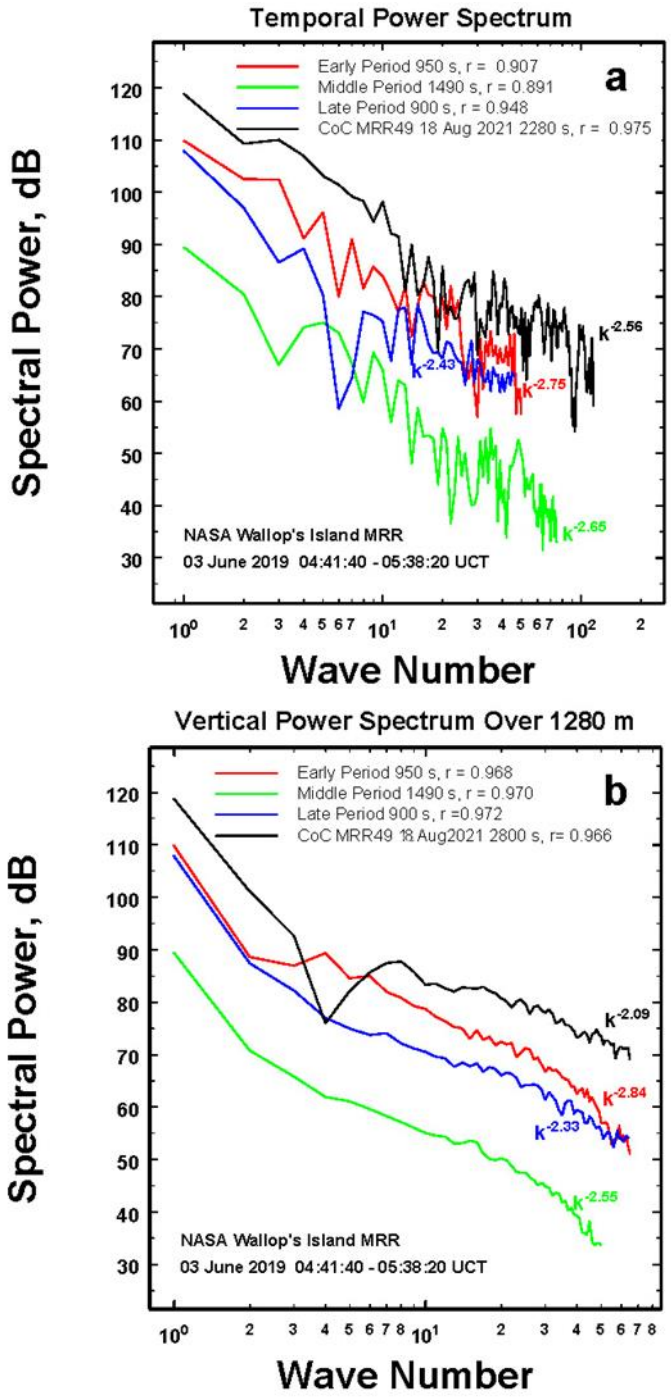

Figure 8. One dimensional power spectra in time (a) and height (b) along with power fits as functions of wave number. In (a), the wave numbers per the different times listed in the legend while it (b) the wavenumbers are per 1280 m.

All of these power spectra can be fit using power functions to a reasonable degree of correlation. Many of the exponents are quite similar regardless of being in the vertical or in the horizontal (temporal) direction. While the vertical axis covers several orders of magnitude, with the exception the horizontal power spectrum of the MRR49 data, the

Preprints (www.preprints.org) | NOT PEER-REVIEWED | Posted: 29 March 2022 doi:10.20944/preprints202203.0373.v1

wavenumbers are shy of the two orders of magnitude required for designating them to be a 'power-law' according to the findings of [18]. On the other hand the general similarity of the various fits suggest that it might be useful to combine the data in the two dimensions.

This is done next by computing the one-dimensional radial spectra regardless of time or altitude as illustrated in Figure 9. This is accomplished here first by converting the temporal axis into a spatial dimension assuming a mean advection speed of 1 m s^{-1}. The 2D horizontal-vertical coordinate system of the original 2D power spectrum by first using the fft2 routine in Matlab® and then multiplying by its complex conjugate. This 2D power spectrum of values at (Δx,Δy)is then converted into 2D polar coordinate system of (Δr,θ) values of the power spectrum so that the radial spectra can then be computed by integrating over all the angles θ for each Δr.

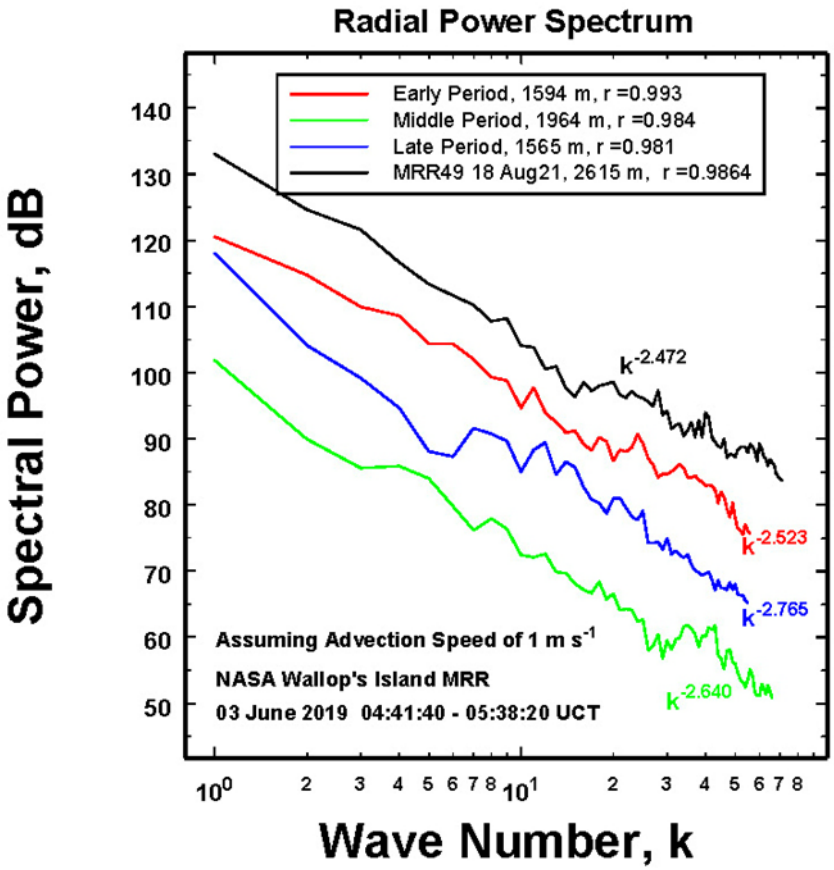

Figure 9. The radial power spectra for the data in Figure 8 with *k* being the wave number for the distances indicated in the legend.

The intercept at $k = 1$ provides a good measure of the total variability of the data at the different times. All of the slopes are quite similar. However, these values are consistently larger in magnitude than many reported in the literature which usually range from 1 – 2 for large horizontal and temporal domains. As [19] point out and as Molini et al. [20] reemphasize, the magnitude of the exponent increases as the time and space scales decrease. For the data here, then, it is not surprising to see larger exponents because the temporal and spatial domains of these measurements are smaller and finer compared to what is normally used. In addition, no other studies have been able to look at the vertical plane in this detail thus complicating any comparisons to previous observations. Consequently, we take these observed slopes at face value within the restrictions just presented.

Preprints (www.preprints.org) | NOT PEER-REVIEWED | Posted: 29 March 2022 doi:10.20944/preprints202203.0373.v1

However, the exact magnitude also depends upon the assumed average advection velocity as illustrated in Figure 10. When the advection velocity is increased to 5 m s^{-1}, the negative slope has

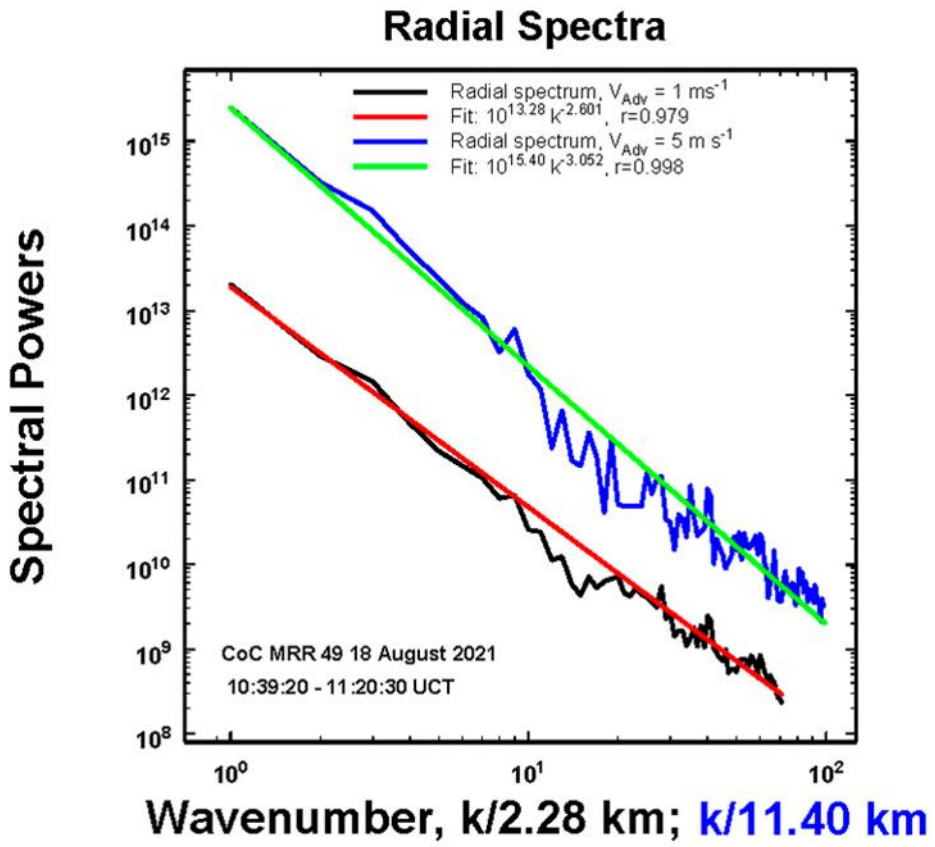

Figure 10. An example of the radial power spectra corresponding to two different assumed advection velocities. The increase in the magnitude of the negative slope is discussed in the text.

increased significantly in magnitude. To see why, consider a particular Fourier wavelength component describing the rain field for the 1 ms^{-1} advection velocity. When this wavelength is instead moving at 5 m s^{-1}, the wavelength is 'stretched' compared to what it was at the 1 m s^{-1} velocity. Or to put it another way, the wavelength increases by a factor of 5 so that the wave number is decreased by a factor of 5. This means that more and more of the spectral energy is moved from shorter toward longer wave lengths so that the radial power spectrum now shows a steeper tilt (negative slope).

This, then, highlights the limitation of trying to convert a time-height profile into representative 2-D spatial data so that ultimately, the statistical analysis of 2-D height distance rainfall data must be based upon using direct simultaneous observations by a line of several vertical pointing radars. As a first step toward this goal and part of current funding, we will be collecting simultaneous measurements using two MRR Pro radars, but, because of extenuating circumstances, have yet to gather such data.

2.2. Lighter, steadier rain

Figure 11 is a plot of the rainfall rate in a winter rainstorm at Wallop's Island, Virginia. Obviously, the rainfall rates during this period are less intense rain than in the previous sets of analyzed data above. For these observations, the peak frequency of occurrence is at 2.7 mm h-1 and a mean rate at 4.7 mm h-1 but with a few embedded regions of more intense rain. Over the entire period, calculations show that IXH = 1.0 so that the data

Preprints (www.preprints.org) | NOT PEER-REVIEWED | Posted: 29 March 2022 doi:10.20944/preprints202203.0373.v1

are statistically heterogeneous. Yet within these data, there is a period of apparent lighter, steadier rain.

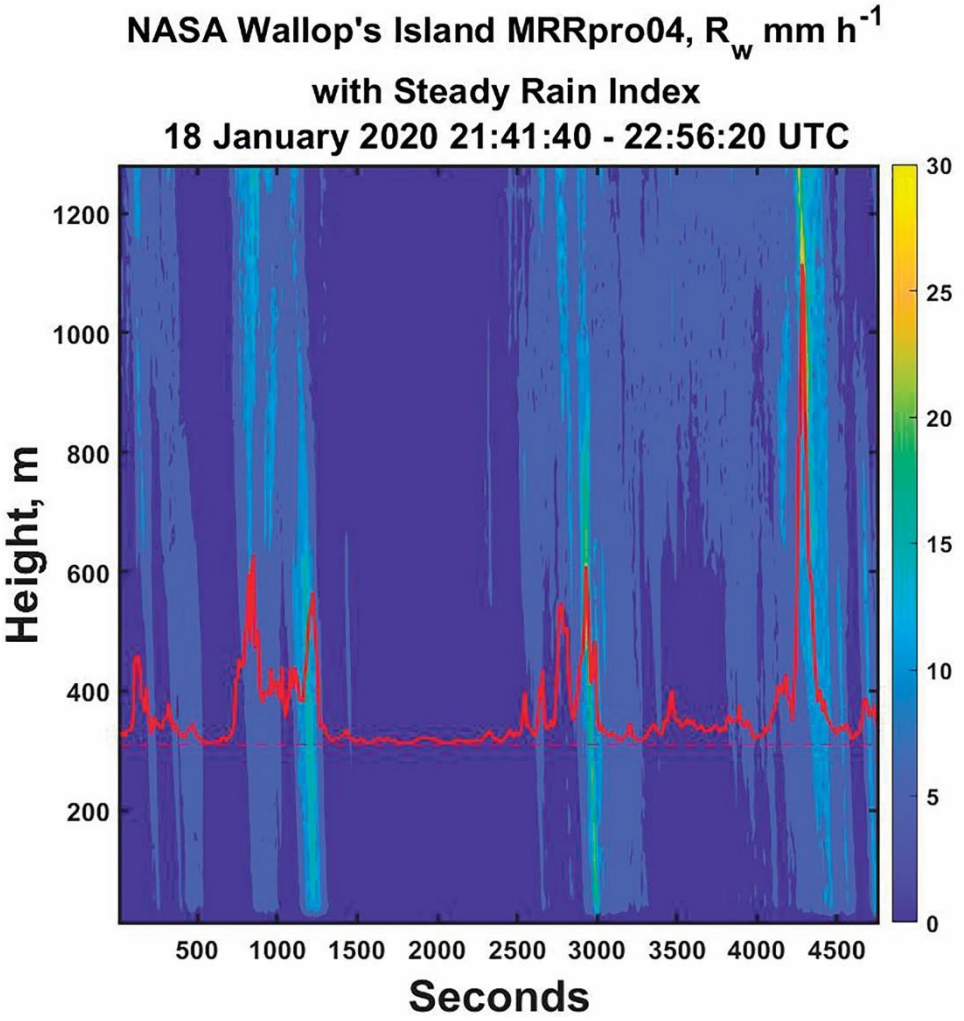

Figure 11. The air velocity corrected rainfall rate during a winter rain event. The red line is the calculated steady rain index with the dashed line denoting perfectly steady rain.

To see whether or not the rain in this region from 1340 – 2390 seconds is truly steady, we use the approach of Jameson and Kostinski [21] to define a steady rain index (*SRIndx*) using their equations (8) and (11) such that

$$SRIndx = \frac{\sigma_R^2}{\sigma_P^2} = 1 + \bar{R}^2 \left[\frac{\sigma_n^2}{\bar{n}^2} - \frac{1}{\bar{n}} \right] \tag{3}$$

where σ^2_P is the variance of the rainfall rate having a Poisson distribution of total number of raindrops n during the observation and a mean rainfall rate, $\bar{R}$, equal to the observed mean rainfall rate, σ^2_R is the variance of the observed rainfall rate during the observation, σ^2_n is the variance of the observed number of drops during the observation, and $\sigma_n^2 = \bar{n}$ is the observed mean number of drops.

There are two ways to calculate these latter quantities. One is to look at the data in height at each time and the other is to look across all times a particular height. It is the former method that makes sense here. The *SRIndx* is plotted as the solid red line in Figure 11. When the rain is steady, the number of drops is Poisson [21], and then *SRIndx*=1 because for Poisson rain $\sigma_n^2 = \bar{n}$. This is indicated by the dashed line in Figure 11.

Preprints (www.preprints.org) | NOT PEER-REVIEWED | Posted: 29 March 2022 doi:10.20944/preprints202203.0373.v1

There is only one 17.5 minute period when the rain can be considered to be really steady between 1340 to 2390 seconds when the solid rain line is very near the dashed. In that location the statistical homogeneity index is found to be 0.10 as well so that these observations may also be considered statistically homogeneous thus allowing the calculation of a correlation function and more general radial power law.

This is illustrated in Figure 12 where an equivalent length radial spectrum for a neighboring statistically heterogeneous data is also plotted. Obviously, in this instance there is a noticeable difference between the two radial spectra thus emphasizing that one cannot just use statistically heterogeneous data as a substitute for statistically homogeneous data. For completeness, from the fit in Figure 12, the corresponding correlation function for the homogeneous data is $\rho(x) = x^{-0.200}$.

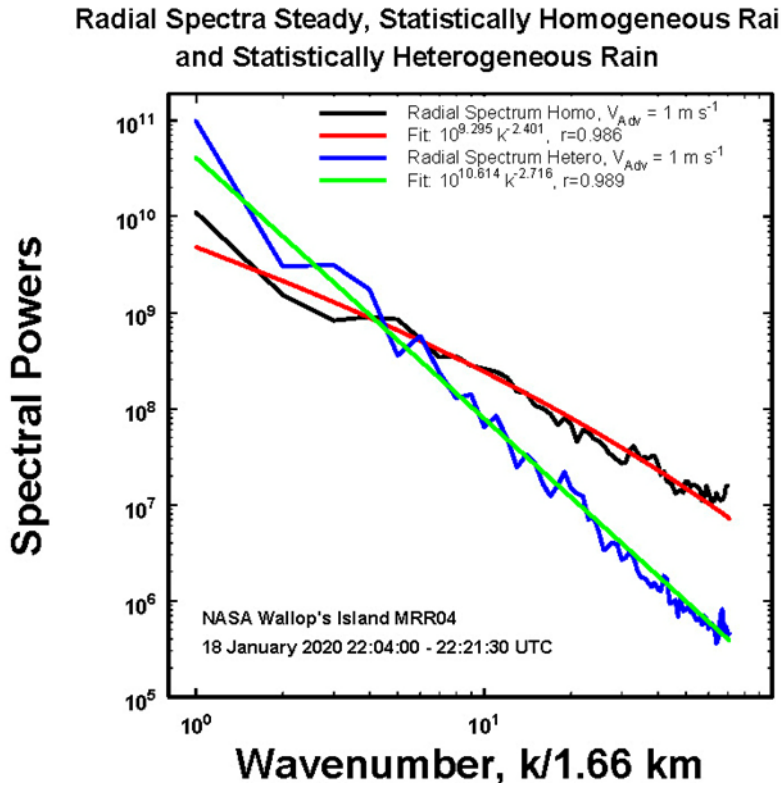

Figure 12. The computed radial power spectrum assuming an advection velocity of 1 m s^{-1} for the period of steady rain and for the next1060 seconds of statistically inhomogeneous, non-steady rain as discussed further in the text.

Nevertheless, in this particular example, for a fixed mean rainfall rate of 50 mm h^{-1} such as might be produced at coarse 5 km resolution by a numerical model or as measured by a radar, that acts to filter out fine scale structures [22,23], we generate two synthetic time series of data from these different radial spectra fits. This is accomplished using the technique of several different investigators (e.g., [24]) in which L complex Fourier amplitudes (A) are created by assigning random phases (φ) to samples of the wavenumbers ($\boldsymbol{k}$) at a fixed interval along L from the fits. That is, the constructed series is

$$A_j = \sqrt{\frac{S_j(k)}{2L\Delta}}\, exp\left(i\varphi_k\right) \tag{4}$$

where S is the fit to the power spectrum. This series is then Fourier transformed and complex conjugated to get a data series consistent with the input spectral power fits.

These curves (Figure 13a) can be interpreted as observations by instruments over a 5 km area at one moment or by one instrument one fixed location in time where the time

Preprints (www.preprints.org) | NOT PEER-REVIEWED | Posted: 29 March 2022 doi:10.20944/preprints202203.0373.v1

would be distance/V_{Adv} where V_{Adv} is the mean advection speed of the rain. Because of the similarity of the two expressions for the spectral power fits, the structures are remarkably similar but there are important differences in magnitudes as reflected in the histograms (Figure 13b).

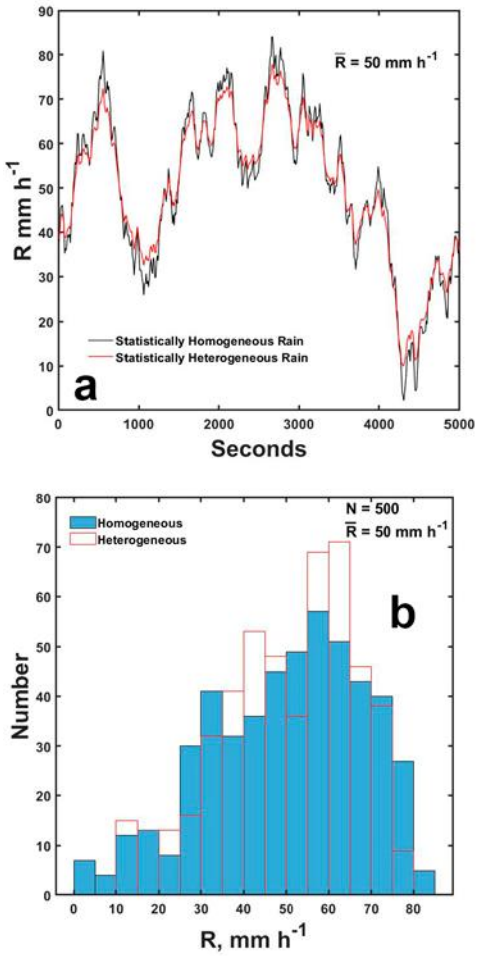

Figure 13. (a)Time series of synthesized data over an 83 minute using the two power spectra in Figure 12 showing real differences between the two (b) histograms for each synthesized rainfall highlighting the differences in (a).

The maximum differences are about 10 mm h^{-1} for the mean R of 50 mm h^{-1} or about 20% with an integrated total absolute difference of 1225 mm h^{-1}. While not huge, such differences could, at times, become significant, for example, when looking at storm run-off or at soil erosion.

While Figure 13a represents what might be seen in time (or a horizontal space of 5 km for a VA_{dv} = 1 m s^{-1}), Figure 14 shows what one realization might look like over a 2 km height not unlike what was observed in some of the data in height at one time presented here.

Preprints (www.preprints.org) | NOT PEER-REVIEWED | Posted: 29 March 2022 doi:10.20944/preprints202203.0373.v1

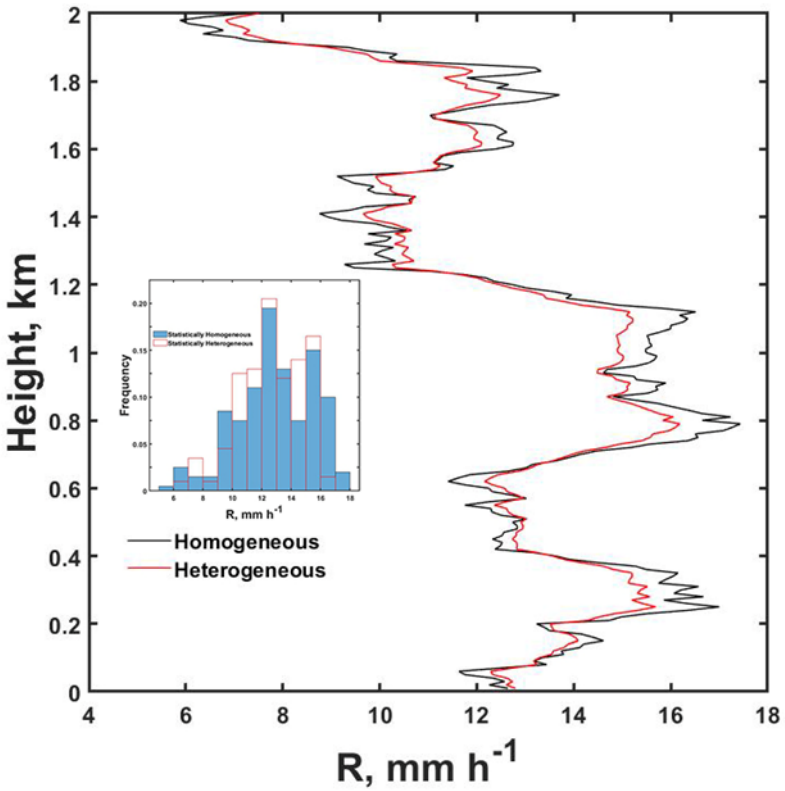

Figure 14. An example of the differences in the rainfall rates for statistically homogeneous and heterogeneous rain in height using the respective power spectral fits.

It also suggests how radar observations of rainfall rate might vary with altitude depending upon the radar beam dimensions and geometry of the observations, of course, as illustrated in Figure 15 for Marshall-Palmer rain [25]. The limit of the X-axis would imply a variation in the radar reflectivity factor of 8 dBZ (a factor of 6) aside from the usual statistical signal fluctuations.

Preprints (www.preprints.org) | NOT PEER-REVIEWED | Posted: 29 March 2022 doi:10.20944/preprints202203.0373.v1

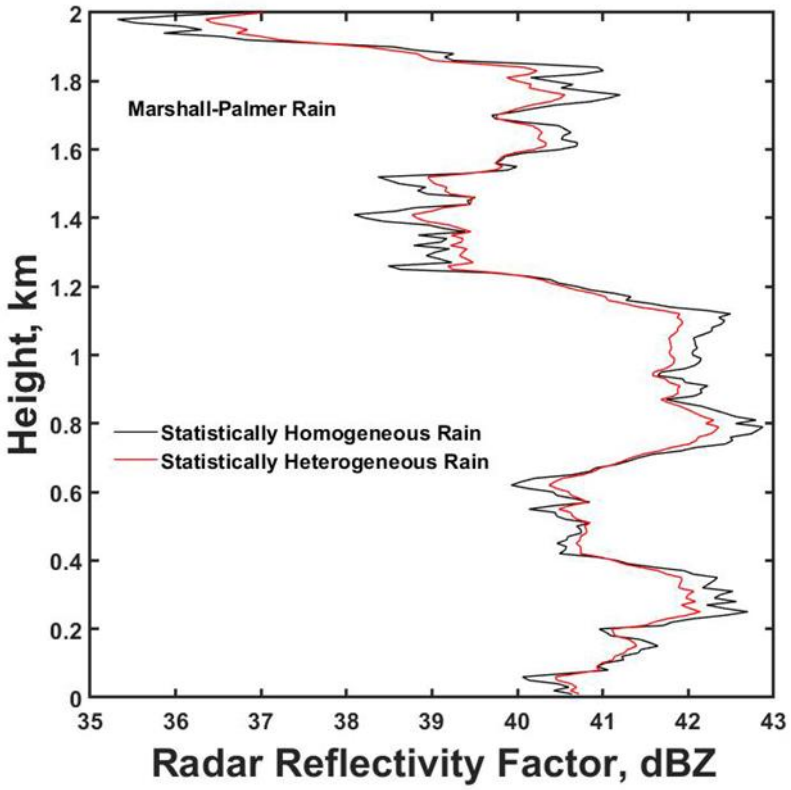

Figure 15. The radar reflectivity values corresponding to the assumption of a Marshall-Palmer rain (Marshall and Palmer 1948) and corresponding to the synthesized rainfall rates in Figure 14.

5. Concluding Remarks

In this paper, fine scale rainfall rates were calculated using Doppler radar measurements properly corrected for vertical air velocity and attenuation. This produced time-height profiles of rainfall rates which could be statistically analyzed over periods of varying length up to 1.28 km height at 10 m/ 10 s resolution for convective types of rain and for one case of less intense, steadier rain. With the exception of one period of steadier rain, the data were all found to be statistically heterogeneous with only very localized pockets of statistically homogeneous rainfall. Consequently, in general it was not possible to construct meaningful correlation functions or to use the Khintchine-Wiener theorem to transform such relations into radial power spectra. Instead it was necessary to directly compute 2-D power spectra using a Fourier transform after first assuming a fixed advection velocity of 1 ms^{-1} so that the temporal axis could be transformed into a spatial axis These, in turn, could be used to compute 1D radial power spectra applicable to each case only.

Nevertheless, in all cases, these radial power spectra could be well fit to the wave numbers by a power relations with negative exponents ranging from 2.47 to 2.76 for both the NASA Wallop's Island MRR observations and those using the College of Charleston MRR radar over a year later and at a different location near Charleston, South Carolina. The precise values, however, are shown to depend upon the assumed advection velocity so that with greater advection speeds, the wavelengths are stretched leading to larger exponents as discussed in the text. Consequently, the only way to get estimates of the true spectral exponents is to collect measurements using spatially separated radars a process being undertaken within current grant.

Nevertheless, in spite of the limitations of the current data, useful conclusions are still possible. For example, based upon these observations and analyses, it appears likely that convective rainfall data will be predominantly statistically heterogeneous. Consequently, rather than looking for universal scaling laws in such precipitation, it will likely be more productive to build a catalog of such relations in a wide variety of rainfall types

at locations where they are to be used in order to better scale either radar rainfall estimates over larger beam dimension above the surface or large scale outputs from numerical forecast models for applications to rain run-off warnings or soil erosion research. Additional general findings are also in process. In particular, this research is being extended to explore the behavior of radial power spectral fits in response to the rainfall rates and to the total spectral powers with some interesting findings to appear in a forthcoming paper currently under preparation.

Author Contributions: There are three authors who contributed to this work, namely A. R. Jameson (AJ), M. L. Larsen (ML). AJ devised and developed this idea, ML provided some of the data associated with the College of Charleston, carefully checked the science and made important suggestions.

Funding: This work was supported (AJ) by the National Science Foundation (NSF) under grant AGS2001343 and by grants AGS201490, 1823334 and 1532977 (ML).

Data Availability Statement The data and Matlab programs are at https://data.mendeley.com/datasets/rfw8h7h2pk/3

Conflicts of Interest: We wish to confirm that there are no known conflicts of interest associated with this publication and there has been no significant financial support for this work that could have influenced its outcome. All of the sources of funding for the work described in this publication are acknowledged above.

References

1. Zawadzki, I. Fractal Structure and Exponential Decorrelation in Rain. *J. Geophys. Res.* **1987**, *92*, 9586, doi:10.1029/JD092iD08p09586.
2. Crane, R.K. Space-Time Structure of Rain Rate Fields. *J. Geophys. Res. Atmospheres* **1990**, *95*, 2011–2020, doi:10.1029/JD095iD03p02011.
3. Georgakakos, K.P.; Carsteanu, A.A.; Sturdevant, P.L.; Cramer, J.A. Observation and Analysis of Midwestern Rain Rates. *J. Appl. Meteorol.* **1994**, *33*, 1433–1444, doi:10.1175/1520-0450(1994)033<1433:OAAOMR>2.0.CO;2.
4. Rodriguez-Iturbe, I.; Marani, M.; D'Odorico, P.; Rinaldo, A. On Space-Time Scaling of Cumulated Rainfall Fields. *Water Resour. Res.* **1998**, *34*, 3461–3469, doi:10.1029/98WR02701.
5. Deidda, R. Rainfall Downscaling in a Space-Time Multifractal Framework. *Water Resour. Res.* **2000**, *36*, 1779–1794, doi:10.1029/2000WR900038.
6. Löffler-Mang, M.; Kunz, M.; Schmid, W. On the Performance of a Low-Cost K-Band Doppler Radar for Quantitative Rain Measurements. *J. Atmospheric Ocean. Technol.* **1999**, *16*, 379–387, doi:10.1175/1520-0426(1999)016<0379:OTPOAL>2.0.CO;2.
7. Jameson, A.R.; Larsen, M.L.; Wolff, D.B. Improved Estimates of the Vertical Structures of Rain Using Single Frequency Doppler Radars. *Atmosphere* **2021**, *12*, 699, doi:10.3390/atmos12060699.
8. Jameson, A.R. On the Importance of Statistical Homogeneity to the Scaling of Rain. *J. Atmospheric Ocean. Technol.* **2019**, *36*, 1063–1078, doi:10.1175/JTECH-D-18-0160.1.
9. Jameson, A.R. A New Characterization of Rain and Clouds: Results from a Statistical Inversion of Count Data. *J. Atmospheric Sci.* **2007**, *64*, 2012–2028, doi:10.1175/JAS3950.1.
10. Jameson, A.R. A Bayesian Method for Upsizing Single Disdrometer Drop Size Counts for Rain Physics Studies and Areal Applications. *IEEE Trans. Geosci. Remote Sens.* **2015**, *53*, 335–343, doi:10.1109/TGRS.2014.2322092.
11. Das, S.; Jameson, A.R. Site Diversity Prediction at a Tropical Location From Single-Site Rain Measurements Using a Bayesian Technique. *Radio Sci.* **2018**, doi:10.1029/2018RS006597.
12. Anderson, A.; Kostinski, A. Reversible Record Breaking and Variability: Temperature Distributions across the Globe. *J. Appl. Meteorol. Climatol.* **2010**, *49*, 1681–1691, doi:10.1175/2010JAMC2407.1.

13. Anderson, A.; Kostinski, A. Evolution and Distribution of Record-Breaking High and Low Monthly Mean Temperatures. *J. Appl. Meteorol. Climatol.* **2011**, *50*, 1859–1871, doi:10.1175/JAMC-D-10-05025.1.
14. Jameson, A.R.; Larsen, M.L.; Kostinski, A.B. On the Detection of Statistical Heterogeneity in Rain Measurements. *J. Atmospheric Ocean. Technol.* **2018**, *35*, 1399–1413, doi:10.1175/JTECH-D-17-0161.1.
15. Jameson, A.R.; Larsen, M.L.; Kostinski, A.B. Disdrometer Network Observations of Finescale Spatial–Temporal Clustering in Rain. *J. Atmospheric Sci.* **2014**, *72*, 1648–1666, doi:10.1175/JAS-D-14-0136.1.
16. Wiener, N. Generalized Harmonic Analysis. *Acta Math.* **1930**, *55*, 117–258, doi:10.1007/BF02546511.
17. Khintchine, A. Korrelationstheorie der stationaren stochastischen Prozesse. *Math. Ann.* **1934**, *109*, 604–615, doi:10.1007/BF01449156.
18. Stumpf, M.P.H.; Porter, M.A. Critical Truths About Power Laws. *Science* **2012**, *335*, 665–666, doi:10.1126/science.1216142.
19. Fraedrich, K.; Larnder, C. Scaling Regimes of Composite Rainfall Time Series. *Tellus Dyn. Meteorol. Oceanogr.* **1993**, *45*, 289–298, doi:10.3402/tellusa.v45i4.14893.
20. Molini, A.; Katul, G.G.; Porporato, A. Revisiting Rainfall Clustering and Intermittency across Different Climatic Regimes: CLUSTERING AND INTERMITTENCY IN RAINFALL. *Water Resour. Res.* **2009**, *45*, doi:10.1029/2008WR007352.
21. Jameson, A.R.; Kostinski, A.B. When Is Rain Steady? *J. Appl. Meteorol.* **2002**, *41*, 83–90, doi:10.1175/1520-0450(2002)041<0083:WIRS>2.0.CO;2.
22. Jameson, A.R. Spatial and Temporal Network Sampling Effects on the Correlation and Variance Structures of Rain Observations. *J. Hydrometeorol.* **2017**, *18*, 187–196.
23. Jameson, A.R. On Observations of Correlation Functions and Power Spectra in Rain: Obfuscation by Advection and Sampling. *Meteorol. Atmospheric Phys.* **2020**, doi:10.1007/s00703-020-00758-x.
24. Cohen, J.E..; Newman, C.M.; Cohen, A.E.; Petchey, O.L.; Gonzalez, A. Spectral Mimicry: A Method of Synthesizing Matching Time Series with Different Fourier Spectra. *CIRCUITS Syst. SIGNAL PROCESS* **1999**, *18*, 431–442.
25. Marshall, J.S.; Palmer, W.M.K. The Distribution of Raindrops with Size. *J. Meteorol.* **1948**, *5*, 165–166, doi:10.1175/1520-0469(1948)005<0165:TDORWS>2.0.CO;2.